Applied Surface Science 670 (2024) 160713

Contents lists available at ScienceDirect

Applied Surface Science

journal homepage: www.elsevier.com/locate/apsusc

Full Length Article

The impact of chemical functionalization of carbon nanotubes on the electrochemical performance of carbon fiber/pyrocarbon/carbon nanotube composites as potential materials for electrodes for nerve cell stimulation

Marcel Zambrzycki [a], Ryszard Wielowski [a], Maciej Gubernat [a], Danuta Jantas [b], Beata Paczosa-Bator [a], Aneta Fraczek-Szczypta [a,*]

[a] Faculty of Materials Science and Ceramics, AGH University of Krakow, Mickiewicza 30 Av., 30-059 Krakow, Poland
[b] Maj Institute of Pharmacology Polish Academy of Sciences, Department of Experimental Neuroendocrinology, Smetna 12 Str., 31-343 Krakow, Poland

ARTICLE INFO

Keywords:
Deep brain stimulation
Neural electrodes
Neurodegenerative disorders
Carbon nanotubes
Carbon-carbon composites
Carbon electrodes
Electrochemical properties
Parkinson's disease

ABSTRACT

In this work, we propose a new carbon–carbon (C–C) composites as a potential materials for electrodes for neural stimulation in neurodegenerative disorders. The C–C composites were made via chemical vapour deposition (CVD) synthesis of pyrocarbon on carbon fibers, with subsequent thermal spray deposition of carbon nanotubes (CNT). Different CNT types were tested to evaluate their impact on electrochemical and biological performance. Materials were analyzed for microstructure, surface chemistry, and electrochemical properties, then tested using SH-SY5Y neuroblastoma cells for biological assessment. The C–C composites coated with a hydroxy-terminated CNT demonstrated significantly enhanced electrochemical properties, in particular increased cathodal charge capacity up to 12.51 mC cm^{-2}, a wide safe potential window of −1.53 to 1.26 V, and decreased impedance, and cut-off frequency ($f_{cut\text{-}off}$ = 0.16 kHz). No acute negative biological responses of the materials were detected after 48 h of exposition. Such properties significantly outperform the properties of platinum, which is the basic element of platinum electrodes, demonstrating the excellent performance of the obtained composites and showing it may constitute the basic element of carbon electrodes for nerve stimulation in the future. Our work presents the method for obtaining biologically inert carbon composite micro-electrodes which can potentially be adapted to neural stimulation.

1. Introduction

Neurodegenerative disorders are conditions leading to gradual and slow neuronal damage in the human brain. The initial phases of these diseases are asymptomatic, and the first symptoms appear after damage to a specific part of the nervous system. As the disease progresses, i.e. as the number of dying neurons increases, the patient's ability to function generally deteriorates, potentially leading to a fatal outcome [1,2]. Neurodegenerative disorders include, among others: Alzheimer's disease, Parkinson's disease, Huntington's disease, amyotrophic lateral sclerosis, multiple sclerosis and others [1,3]. Approaches to address neurodegenerative disorders focus on alleviating symptoms and slowing down the progression of the disease. Treatment methods include pharmacological and surgical treatments. In the case of Parkinson's disease, the pharmacological treatment is based on replenishing the dopamine levels, inhibiting the breakdown of this transmitter in the brain or providing the body with substances that stimulate dopamine receptors. The drug most often administered in Parkinson's disease is levodopa, which is a precursor of dopamine. However, the advanced stage of the disease may make drug treatment ineffective or may cause undesirable side effects [4]. Then, surgical treatment methods are used, including deep brain stimulation (DBS), which involves implanting thin electrodes into deep parts of the brain [5,6,7]. The electrodes are connected via wires to the stimulator located in the chest. The use of DBS is aimed at modulating pathological neural circuits [6]. Implanted electrodes transfer electrical impulses generated by a stimulator (pulse generator) placed in the patient's body as a constant source of current [8]. The most commonly used materials for electrodes for stimulation of neural tissue are metals such as platinum or platinum-iridium alloys [5,9,10]. Some of the major problems after the implantation of currently used electrodes including metallic electrodes are hemorrhage, edema, and a foreign body reaction, leading to the formation of glial tissue around the

* Corresponding author.
E-mail address: afraczek@agh.edu.pl (A. Fraczek-Szczypta).

https://doi.org/10.1016/j.apsusc.2024.160713
Received 28 March 2024; Received in revised form 3 July 2024; Accepted 8 July 2024
Available online 9 July 2024

electrodes, increasing the impedance between the tissue and the electrode, requiring the use of higher voltages and currents [9,10]. However, the higher the voltage and currents used, the greater the risk of heating the tissue surrounding the electrode and inducing undesirable electrochemical reactions. Furthermore, the mismatch of stiffness and hardness between the metal and the tissue also has a significant impact on the formation of scar tissue [11,12]. Miniaturization of stimulating electrodes may reduce tissue damage and stimulate precisely defined areas of the brain. Therefore, new solutions are constantly being sought, in terms of miniaturization of electrodes and materials, extending the life of electrodes, and the safety of their use in tissue [5,13]. Various material solutions appear in the literature, based primarily on the modification of the surface of classic metallic electrodes with oxides, carbon layers, conductive polymers or various types of composites [12,13,14,15,16,17]. Research to date shows the possibility of using carbon fibers (CF) as a material for stimulation and recording electrodes, for the detection of neurotransmitters, and monitoring signals of the nervous system [14,18,19,20,21]. Due to a number of advantageous properties such as high electrical and thermal conductivity, corrosion resistance, low density, and flexibility, carbon materials are an interesting alternative to classic electrodes, allowing minimization of the drawbacks of metal materials [10,21,22,23,24]. Despite the above, the electrochemical capacity of many carbon materials e.g. carbon fibers is insufficient to be used as the sole material of electrodes for stimulation of nerve cells [23,25]. The use of carbon fibers as an alternative to metal electrodes in DBS also requires a certain stiffness to allow them to be inserted into deeper areas of the brain. One of the solutions may be the use of electrode materials based on a C–C composite, which allows, on the one hand, stiffening of the material, and at the same time reduction of the electrode diameter below 500 μm [23,25,26]. A small electrode is associated with high electrochemical impedance due to the limited surface area available for the interaction with the liquid. As a result, higher voltages are needed to drive the current through the interface, increasing the risk of electrochemical side effects such as corrosion or electrolysis. Therefore, research on CF electrodes focuses on their modification using other carbon materials, such as carbon nanotubes (CNT), graphite, or diamond, to lower impedance and increase the safe charge injection capacity (CIC), allowing for increased stimulating capabilities [24,27,28]. The introduction of high surface area coatings improve the performance of the electrodes by increasing their electrochemically active surface area, therefore in this context, carbon nanomaterials such as CNTs may be of great importance [29,30,31]. An example of CNT-based carbon materials with potential use for stimulating cells of the nervous system are CNT yarns, which have satisfactory electrochemical properties, including a high charge storage capacity (CSC) value [22,32,33,34,35]. However, despite progress, the methods of obtaining them are not easy [36,37,38,39]. In the case of these materials, as in the case of carbon fibers, there is a problem of insufficient stiffness to penetrate deeper brain regions despite their high mechanical properties. From this point of view, it seems reasonable to search for other methods of obtaining carbon-based electrode materials. The solution proposed in this work is innovative because it combines the features of three carbon materials, namely carbon fiber, pyrolytic carbon (PyC) and CNT. The first of them gives the composite directionality and mechanical strength. The second one is a matrix that stiffens the composite and makes it surgically handy, and at the same time has hemocompatible properties confirmed in the literature [40,41,42], which may have an additional positive meaning in the proposed application. The third and last phase, i.e. CNT, has high electrochemical properties, which can be additionally modified by chemical treatment [32].

In such electrodes, during the electrical stimulation, short pulses of current are injected into the tissue through the contact surface, which physically form the electrode–electrolyte interface. In practice, the pulses must cross the solid–liquid interface to reach the cell membrane, which means that a transition from electronic to ionic signal transmission must occur [43]. Therefore, electrochemical studies are the key tests to assess the effectiveness and safety of using electrode materials to stimulate neural tissue cells. Recently, Boehler published guidelines for standard in vitro electrode performance tests that should be performed to evaluate the potential of stimulation and recording electrode materials [43]. Standard measures for the charge injection capacity (CIC) and charge storage capacity (CSC) are recommended for stimulation electrodes, describing the capability of a particular materials to safely deliver charge at the electrode/electrolyte interface [43,44,45]. For the determination of the above, fast biphasic current pulsing and voltammetric measurements are used. In turn, for the recording electrodes, the most important parameters include the impedance and cut-off frequency $f_{cut\text{-}off}$, describing the ability of the electrode to accurately sample signals while minimizing its impact on the recorded information [43].

The main goal of this work was to create composites as a potential electrodes fully based on carbon materials, which would constitute an alternative to metallic electrodes classically used in the area of stimulation of neural tissue, and at the same time combining the beneficial features of three carbon materials. As a result of this investigation, innovative composite materials based on carbon fibers and pyrolytic carbon (PyC) were created, which, thanks to surface modifications with various types of CNTs, allowed us to obtain carbon composite rods with electrochemical characteristics exceeding platinum, used as the basic material for DBS electrodes. The obtained materials were characterized by improved charge injection capabilities due to the increased double layer capacitance, and lowered impedance and cut-off frequency, which evidenced enhanced stimulation-recording characteristics of the electrodes. As part of the study, we investigated the effect of chemical treatment of CNT aiming at introduction of functional groups, on the electrochemical and biological performance of carbon based electrodes. Up to this date, there is no information in the literature about electrodes of this type or how to obtain them, and particularly about the method of surface coating of the C–C composite electrodes with CNT. The carbon materials as a potential electrodes were subjected to a number of comprehensive electrochemical, structural and microstructural analyses, which have been supported by in vitro biological tests of cytotoxicity in contact with human SH-SY5Y neuroblastoma cells.

2. Materials and methods

2.1. Materials

Composite materials have been manufactured on the basis of a high-modulus carbon fiber (CF), carbon pyrolytic (PyC) matrix, and various types of multiwalled carbon nanotubes (MWCNT). Dog-bone shape cross-section PAN-based carbon fibers Celion 80 – GY80 (Celanese Co. – presently BASF, USA) were used as the core of the nanocomposite carbon rods [46]. The mean larger and smaller diameter of fibers were 12.4 μm and 4.4 μm, respectively [26]. The matrix of carbon–carbon (C–C) composite was synthesized from a CH_4, and nitrogen was used as a carrier gas (Air Liquide S.A.). MWCNT were used to modify the surface of the composites in each case. The multiwalled carbon nanotubes in the powder form and dispersed (7.5 % MWCNT) were purchased from Nanostructured & Amorphous Materials, Inc., USA. Acetone and ethyl alcohol (Avantor Performance Materials Poland S.A.) were used as dispersion media for the preparation of carbon nanotube suspensions for spray coating. Dulbecco's Modified Eagle Medium (DMEM), fetal bovine serum (FBS) and FluoroBrite™ DMEM used in biological tests were obtained from Gibco (Invitrogen, Paisley, UK). Cytotoxicity Detection Kit was acquired from Roche Diagnostic (Basel, Switzerland), and penicillin, streptomycin, trypsin and ethylenediaminetetraacetic acid (EDTA) were purchased from Sigma-Aldrich, Germany.

2.2. Methods

2.2.1. Characterization of carbon nanotubes

The specific surface area was measured using the ASAP 2020 Plus 2.0

(Micromeritics Instr.) surface area and porosimetry system. Physical adsorption isotherms of nitrogen were recorded, and specific surface area was estimated using the Brunauer–Emmett–Teller (BET) isotherm method. Three measurements were made for each sample, from which the mean value and standard deviation (±SD) were determined. The - obtained data were processed with original software provided with the ASAP 2010 v5.03 instrument.

The CNTs particle size distribution was measured using the dynamic light scattering (DLS) method with a Zetasizer Nano-ZS (Malvern Instr. UK).

In order to assess stability of the CNTs suspensions a zeta potential ξ was measured using the Zetasizer and the folded capillary cell. Both measurements were performed at 25 °C in the diluted suspensions of a given CNT and mixture of solvents used for the spray coating i.e.; 62.6 % pure ethanol, 20.8 % acetone and 16.6 % distilled water. Prior to the DLS and the zeta potential measurements the suspensions were dispersed for 5 min with an ultrasonic processor (VCX 500, Sonics, USA). In both cases the results are an average from three measurements. Three measurements were made for each sample, from which the mean value and standard deviation (±SD) were determined. The obtained data were analyzed with Zetasizer Software 7.02.

The morphology and structure of carbon nanotubes before and after functionalisation were evaluated using a transmission electron microscope FEI Tecnai TF20 X-TWIN (FEG) at an accelerating voltage of 200 kV. Imaging was performed in the bright field (BFTEM) and high resolution (HRTEM) modes. The results were analyzed using a Gatan DigitalMicrograph 3.20.1314.0.

2.2.2. Characterization of C–C composites

The examination of the microstructure and morphology of C–C composites before and after modification with CNT was performed using a scanning electron microscope (SEM) Apreo 2S (ThermoFisher - Scientific, Netherlands). The acceleration voltage was 5 kV.

The Raman spectra of composites were registered using a WITec Alpha 300 spectrometer working with a 488 nm diode laser and a 100x Zeiss magnifying lens. The spectra were collected in the range of 110–4000 cm^{-1}, and each measurement consisted of 3 accumulations and a 30 s integration time. Every sample was measured 3 times and averaged. The recorded spectra were processed with Fityk 1.3.1 software, and the pseudo-Voigt function was used for fitting and deconvolution of the peaks [47].

The chemical state of the surface of the composites after the modification with CNT was determined using the X-ray photoelectron spectroscopy (XPS) spectroscope PHI5000 VersaProbe II Scanning XPS system equipped with an Al radiation source (Kα line, 1486.6 eV). The estimated depth of analytical information was about 5 nm, and the area of analysis was about 100 μm. The spectra were calibrated assuming the binding energy of C1s level = 285 eV, and the background was subtracted using the Shirley method. Peak fitting and processing of obtained data was performed using PHI MultiPak software 9.9.2.

Electrochemical measurements were conducted with the Autolab General Purpose Electrochemical System (AUT302N.FRA-2-AUTOLAB) using a three electrode set-up: Ag/AgCl/3M KCl reference electrode, Pt auxiliary electrode, and carbon nanocomposite rods with a restricted working surface area as an experimental working electrode (l = 5 mm, d = 0.25 mm). Moreover, a Pt wire with the same diameter and contact area was used as a control sample for carbon electrodes. Measurements were carried out in artificial cerebrospinal fluid containing 0.148 M NaCl, 3.0 mM KCl, 1.4 mM $CaCl_2x2H_2O$, 0.8 mM $MgCl_2x6H_2O$, 0.8 mM $Na_2HPO_4x7H_2O$ and 0.2 mM $NaH_2PO_4xH_2O$ dissolved in distilled water. The impedance spectroscopy measurements were performed in the frequency range of 1 to 10^5 Hz, with an amplitude of 10 mV, and a voltage bias of 0.5 V. The fitting of spectra was performed using Nova 2.1.4. software. Cyclic voltammetry (CV) measurements were performed at a scan rate of 100 mV s^{-1}, and the cathodic charge storage capacity (CSC_c) of the tested electrodes was determined as a time integral of the cathodic current density at the range of water window potentials, excluding the extreme peaks attributed to electrolysis of water [21]. Three to four measurements were made for each sample, from which the mean value and standard deviation (±SD) were determined.

2.2.3. Preliminary in vitro study

The human SH-SY5Y neuroblastoma cells (ATCC, passage 12) were cultured as described elsewhere [48]. Cells were maintained in DMEM supplemented with 10 % heat-inactivated FBS and 1 % penicillin/streptomycin solution at 37 °C in an atmosphere containing 95 % air and 5 % CO_2 with saturated humidity. After reaching an 80 % confluence, cells were trypsinised (0.05 % Trypsin/EDTA), counted (Bürker chamber), and seeded at a density of 8×10^4 cells in 350 μL of cell culture medium per well into 48-well plates containing UV-sterilized materials (11 types). Each experimental group consisted of 3 replicates. The impact of the materials on cell viability was estimated after 24 h (Lactate dehydrogenase (LDH) release assay) and 48 h (LDH release assay, light microscopy) of incubation when compared to control groups (wells without any material, cells growing on a polystyrene surface).

The cytotoxicity of materials was assessed by measuring the level of LDH released from cells into the culture media with a Cytotoxicity Detection Kit (Roche) [48]. 24 and 48 h after cell seeding on materials, 50 μl of cell culture supernatant from each experimental well were collected in 96-well plate followed by the addition of a mixture of Cytotoxicity Detection Kit reagents (25 μl/well) for 15 min at RT. The absorbance was measured in a multiwell plate-reader (Infinite® M200 PRO, Tecan, Switzerland) at 490 nm. The data after the subtraction of blank values (cell culture medium) were normalized to the control group and are presented as the mean ± SEM of three wells per group.

The differential interference contrast (DIC) images were taken for each experimental group in triplicates after 48 h of cell incubation using an inverted microscope (AxioObserver, Carl Zeiss, Jena, Germany) equipped with a 10× objective and digital black-white camera (AxioCamMRm, Carl Zeiss, Jena, Germany).

2.2.4. Statistical analysis

The obtained data were analyzed using Statistica software. The analysis of variance (one- or two-way ANOVA) and a post hoc Duncan test for multiple comparisons were used to show statistical significance with an assumed $p < 0.05$.

2.3. Fabrication of C–C composites

2.3.1. Synthesis of CF/PyC composites

The chemical vapour deposition (CVD) method with direct electrical heating of carbon fibers was carried out in a CFCPP-1100 device, Carbon Fiber Pyrolytic Carbon Coating, by Fine Instruments, Poland. The system includes a quartz glass reactor, a CF bundle assembly system, a vacuum pump, the DC generator, a gas exhaust and supply system, flow meters, gas cylinders, and a pyrometer that control the temperature of the fiber bundle. Gasses were supplied directly to the system with the appropriate flow rate. This method was used by us for synthesis of C–C composites in our previous work [26]. For the synthesis, a bundle of CFs weighing 0.68 ± 0.07 mg, which corresponds to approximately 90–110 individual fibers, was placed between the graphite assembly and heated up to 1120 °C by applying current up to 2.4 A. Prior to each synthesis, the air in the reactor chamber was removed using a vacuum pump, and replaced with nitrogen. Subsequently, a mixture of methane and nitrogen (flow rate 2:10 l/h) was introduced into the reactor for 120 s, and after that a pure nitrogen flow was left for another 60 s. Thereafter, CF/PyC composite samples of 1.42 ± 0.19 mg were obtained, which resulted in approx. 48.3 % contribution of the carbon fiber and 51.4 % of the pyrolytic carbon matrix phase.

2.3.2. Chemical functionalization of carbon nanotubes

The type and concentration of surface functional groups can significantly influence the biological and electrochemical performance of carbon materials. In order to investigate this effect, three types of carbon nanotubes with different surface chemistry were tested: non-modified carbon nanotubes without additional functional groups – CNT; oxidized carbon nanotubes with hydroxyl/carboxylic groups – CNT-OH; and amidized carbon nanotubes – CNT-NH. The CNT-OH were obtained by chemically oxidizing CNT in a mixture of concentrated H_2SO_4 and HNO_3 (3:1 vol), according to the procedure described in previous works [49,50]. The amidized carbon nanotubes CNT-NH were prepared by treatment of the as-obtained CNT-OH with ethylenediamine, details of this procedure can be found in [50]. The final products were centrifuged, washed in ethanol, and dried under vacuum.

2.3.3. Preparation of carbon nanotube dispersions

The non-functionalized carbon nanotubes, CNT-OH and CNT-NH were dispersed in a mixture of 62.6 % pure ethanol, 20.8 % acetone, and 16.6 % distilled water [51]. The concentration of carbon nanotubes was 3 mg ml^{-1}. The suspensions were sonicated with an ultrasonic processor (Vibra-cell VCX 130, USA) with an output power of 10–11 W. A single run lasted 5 min, and the sonication treatment was repeated 10 times. The pauses during the sonication were introduced in order to reduce the overheating of the suspensions and avoid possible degradation of the nanomaterials.

2.3.4. Thermal spray coating

A thin layer of CNT was applied to the surface of carbon rods by the thermal spray coating technique using a Fengda airbrush, model BD-134 K. The pressure used during the process was set at 1.2 bar, and total deposition time was 240 s for each C–C composite. The temperature of the heating plate was 300 °C. The preparation procedure (Fig. 1) obtained four types of C–C samples: reference composite rod without CNT layer – CF/PyC; and composites coated with various CNT types – CF/PyC/CNT, CF/PyC/CNT-NH, and CF/PyC/CNT-OH. The photographs of CF/PyC composite rods under and without deformation are shown at Fig. 2 X.

3. Results and discussion

3.1. Characterization of carbon nanotubes

Carbon nanotubes before and after functionalization in the mixture of acids and ethylenediamine were characterized in terms of basic parameters that may affect their biological and electrochemical properties. The morphology and structure of carbon nanotubes were evaluated using transmission electron microscopy in bright field and high resolution modes. Representative images are shown in Fig. 3. The observations showed that the nanotubes had multiple walls, and were characterized by average diameters of 14–27 nm. All types of CNT were well separated, and no major agglomerates were found. The high resolution imaging revealed that the chemical treatment of nanotubes, apart from the introduction of oxygen and nitrogen functional groups, led to the disruption of the near-surface structure, exposing the edge-planes of the CNT walls. In pristine, non-functionalized CNT, the graphene planes building the walls were arranged parallel to the axis of the nanotubes (Fig. 3 G). In turn, after the chemical treatment, the arrangement of graphene planes in near-surface areas of the walls was disrupted in the case of both CNT-OH, and CNT-NH. These exposed edge planes are a source of micropores and defect sites. These, being electrochemically active sites, can enhance the catalytic and capacitive properties of C–C composites. Furthermore, the measurements of interplanar distance d_{002} revealed that it slightly increased after the functionalization, which is consistent with the observed disruption of the CNT plane arrangement: CNT: $d_{002} = 0.3416$ nm; CNT-OH: $d_{002} = 0.3418$ nm; CNT-NH: $d_{002} = 0.3449$ nm.

The specific surface area of nanotubes was examined using the BET isotherm method. The analysis showed significant differences in the surface development depending on the type of functionalization of CNT (Table 1). The lowest value of specific surface area (SSA) was obtained for the non-functionalized CNT – 84.0 $m^2\,g^{-1}$, CNT-NH had SSA = 143.1 $m^2\,g^{-1}$, and CNT-OH were characterized by the highest SSA of 508.3 $m^2\,g^{-1}$. In general, the specific surface area of carbon nanotubes depends on a number of parameters, such as diameter, length, the presence of micro- and *meso*-porosity, tendency towards agglomeration, etc. [52]. In our case, the increased surface area of nanotubes was mainly caused by the disturbed morphology and structure of nanotubes induced by the strong oxidizing agents used, which can cut, introduce

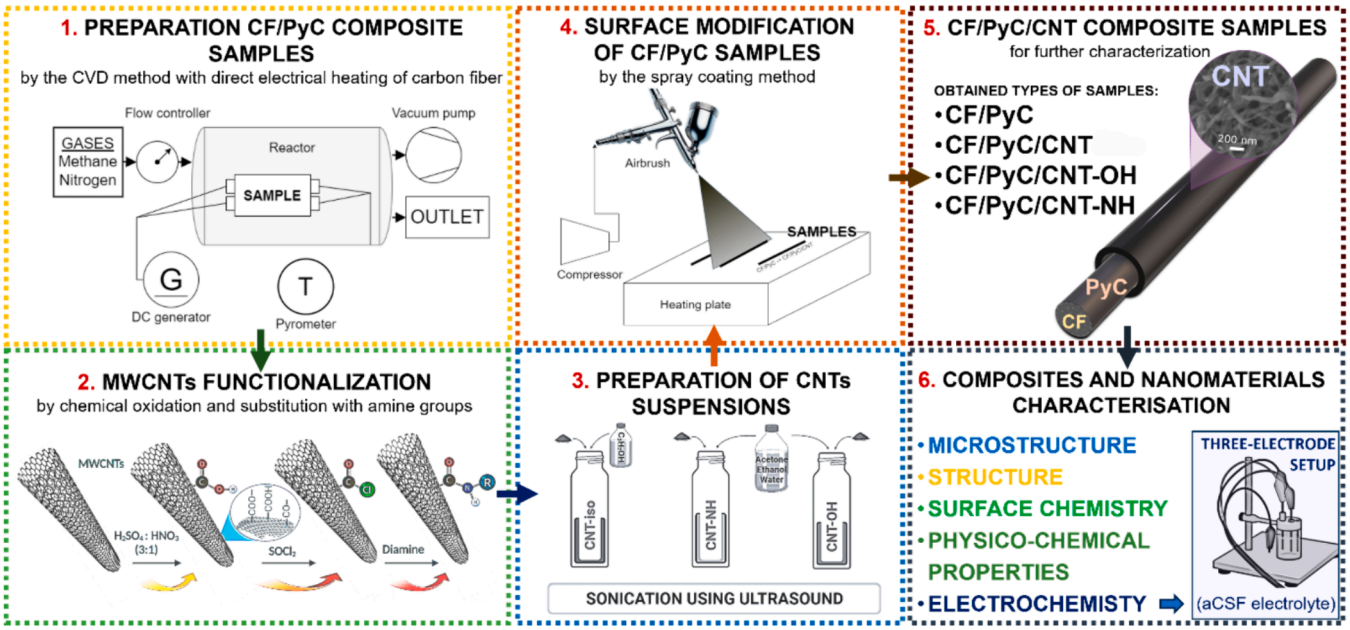

Fig. 1. Scheme for obtaining CF/PyC/CNT composites in form of rods.

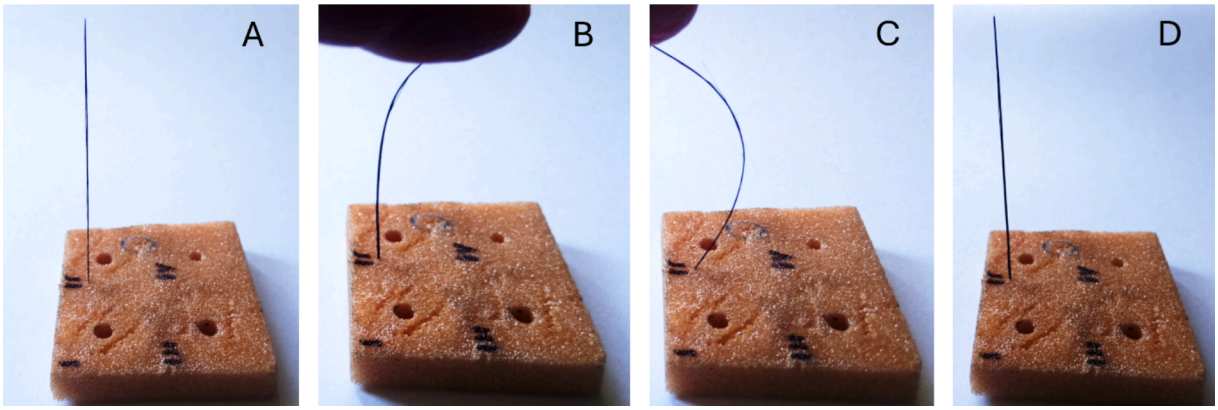

Fig. 2. CF/PyC composites before deformation (A), during deformation (B, C) and after deformation (D).

defects, and make pores into the sidewalls of the CNT [53]. Furthermore, the –OH, –COOH, and –NH polar surface functional groups facilitate dispersion, and prevent agglomeration of CNT, therefore, also acting as a factor potentially increasing the available surface area.

The pristine, and functionalized CNT were used for preparing suspensions for the spray coating of C–C composites, and thereafter the zeta potential ξ was determined in order to assess the stability of the obtained dispersions. The CNTs suspensions were stabilized using solely the electrostatic method based on the electrical charge present at the nanoparticles surface and the formation of the electrical double layer (EDL). Particles of the same type are charged in the same way and repel one from another. In this case, a measure of the electrical charge magnitude is an absolute value of the zeta potential, which is determined at the slip plane within the EDL.

It is generally assumed, that for the good stability of suspensions, an absolute value of the zeta potential should be higher than 30 mV.

The absolute value of this parameter showed trends similar to the specific surface area of nanotubes, namely, the zeta potential was the highest for the functionalized nanotubes: −29.8 and −21.4 mV for CNT-OH, and CNT-NH, respectively, while for the pristine CNT it was only −11.8 mV. The observed differences in zeta potential were directly mirroring the polarity of functional groups on the surface of CNT, namely stronger polarity of –OH bonds as compared to amine bonds. The obtained absolute values of ξ potential suggest good stability of only the CNT-OH dispersion (ξ potential ∼ 30 mV), nonetheless, all inks, including those based on CNT-NH and CNT were stable right after the sonication and also during the deposition process [54]. The suspensions were also characterized using the DLS method, and the obtained hydrodynamic particle size distributions are shown in Fig. S1. The tests showed the significant differences between the suspensions of carbon nanotubes before and after the functionalization. The nanotubes subjected to chemical treatment exhibited significantly smaller mean particle sizes around 165 nm, as compared with 350 nm for pristine CNT, which may have resulted from the cutting of CNT induced by strong acids, and sedimentation of longer nanotubes during the centrifugation process.

3.2. Characterization of C–C composites as potential electrodes

3.2.1. Physicochemical properties

3.2.1.1. Scanning electron microscopy. The microstructure of the obtained C–C composites before and after the modification with CNT was examined using SEM, and the collected images are shown in Fig. 4. The surface of the blank CF/PyC composite was rough and contained numerous globular protuberances characteristic of pyrocarbon (Fig. 4) [55]. The morphology of these precipitates depend strictly on the conditions of PyC synthesis, which was described in detail in our previous work [26]. The applied spray deposition resulted in the formation of a continuous layer of CNT on the surface of CF/PyC in the case of all samples, however, the resulting microstructure differed depending on the type of nanotubes used. In the case of CF/PyC/CNT, the nanotube layer was the roughest and contained numerous spherical agglomerates, which were not observed for CNTs after the functionalization. In the case of CF/PyC/CNT-OH and CF/PyC/CNT-NH composites, the obtained layers were smooth and homogeneous, the surface of CF/PyC/CNT-OH seemed to be the most compact when compared to other composites. The SEM images also suggest that CF/PyC/CNT-OH exhibited the lowest surface microporosity relative to other samples. Achieving lower microporosity and more smoothness of the layer was possible due to better dispersion of CNT-OH in the solvent mixture, due to the presence of functional groups and the shorter dimensions of nanotubes, as evidenced by the results of zeta potential and DLS tests (Table 1 and Fig. S1). Moreover, the presence of oxygen groups on the surface of the CNT-OH may also contribute to a stronger interaction between the nanotubes in the layer.

3.2.1.2. Raman spectroscopy. Raman spectroscopy was performed in order to assess the structural changes of C–C composites after the applied spray deposition with various types of carbon nanotubes (Fig. 5). Spectra of all composites were characterized by the presence of bands characteristic for sp^2 carbon materials – the D band around 1350 cm^{-1}, the G band at about 1590 cm^{-1}, the weak shoulder D' band at 1620 cm^{-1}, the 2D second order band at around 2680 cm^{-1}, the D + G band at 2920 cm^{-1}, and the 2G band at 3210 cm^{-1}. The G band, characteristic for sp^2 carbons, originates from the in-plane tangential stretching of the C=C bonds. The D band indicates the presence of defects that break the translational symmetry of the graphene sheet, and is related to the presence of disordered and amorphous carbon. The D' band is a shoulder peak of the G band, and is due to defect-sensitive resonance effects involving phononic vibrations around the center of the Brillouin zone. Bands 2D, D + G, and 2G lying at higher Raman shifts are attributed to the second order vibration modes [56,57,58].

The unmodified CF/PyC composite was characterized by a spectrum typical of low-structured pyrolytic carbons, and the deposition of CNT caused significant changes in the intensity and positions of the D, G, and D' bands [26]. The ratio of integral intensity of the D and G bands (A_D/A_G) was used as a parameter quantitatively describing the variations in the disordering of the structure of carbon composites (Fig. S2, Table S1). The CF/PyC composite modified with pristine CNT was characterized by the lowest A_D/A_G value of 0.63, which can be attributed to the highly ordered structure of non-functionalized carbon nanotubes. The CNT-OH and CNT-NH modified samples were characterized by higher values of A_D/A_G of 1.19 and 0.82, evidencing the disturbed structure of the carbon nanotubes after the chemical treatment. The high intensity of the D band in these samples was caused by an increased population of defects

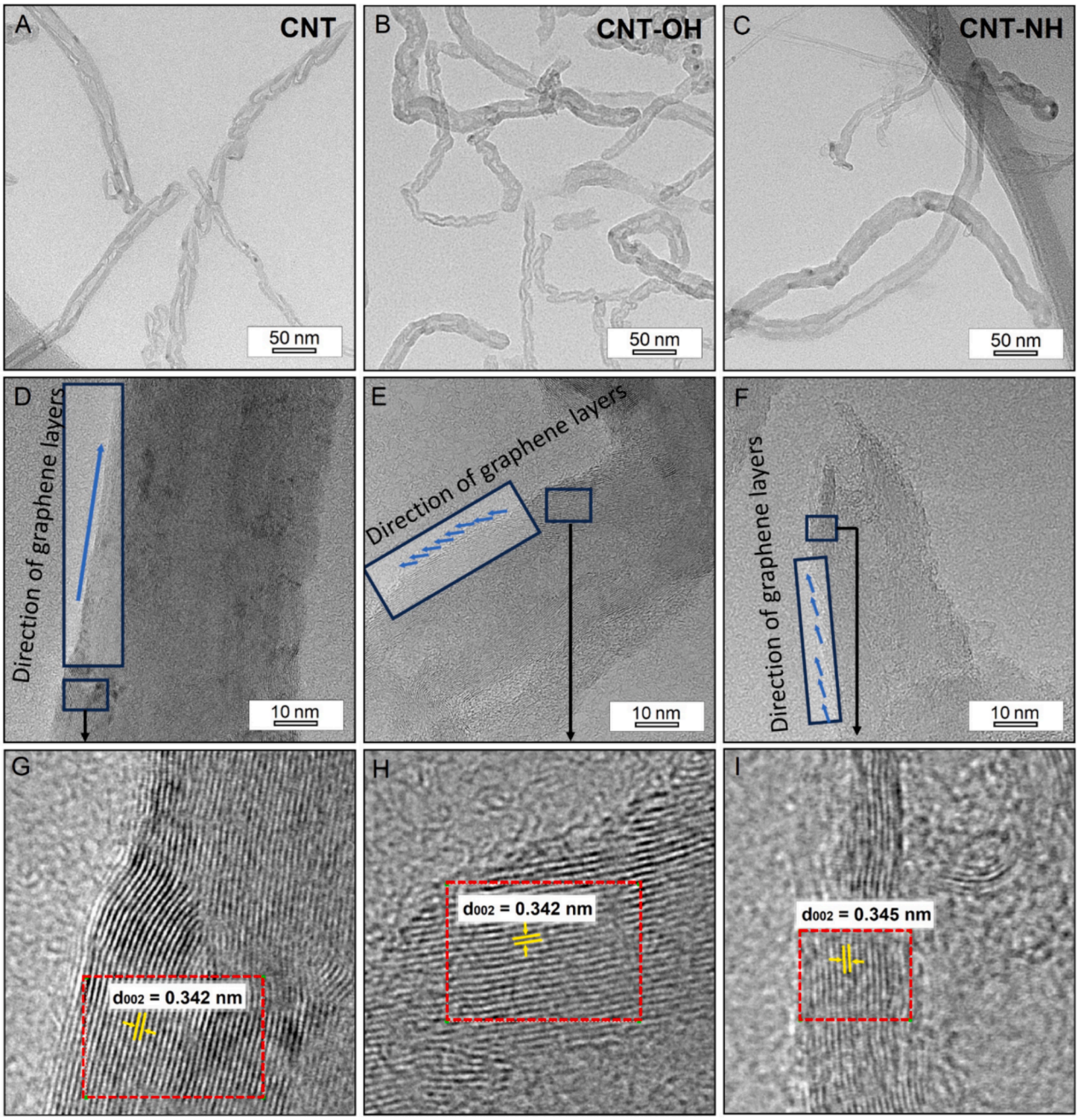

Fig. 3. BFTEM and HRTEM images of CNT (A, D, G), CNT-OH (B, E, H), and CNT-NH (C, F, I).

Table 1
BET specific surface area and zeta potential of carbon nanotubes before and after modification. The data are presented as the mean ± SD from n = 3 for each type of sample.

Sample	Specific surface area (BET) [m^2/g]	Zeta potential ξ [mV]
CNT	84.01 ± 0.26	−11.8 ± 3.4
CNT-OH	508.30 ± 1.05	−29.8 ± 2.4
CNT-NH	143.14 ± 2.72	−21.4 ± 0.9

formed on the sidewalls and tips of the nanotubes, which were oxidized as a result of the action of a strong oxidizing medium (mixture of H_2SO_4 and HNO_3) [5759]. During the oxidation of CNTs, not only are defects formed on the surfaces of the sidewalls and ends of the nanotubes, but the destruction of the graphitic integrity and the subsequent formation of small graphitic fragments may also occur, which also contributes to the increase in the D band. In the case of NH-modified nanotubes, their modification was a multistage process involving functionalization in a mixture of $SOCl_2$:DMF for 24 h, washing with tetrahydrofuran and functionalization in $C_2H_4(NH_2)_2$, all of which may lead to an appreciable elimination of the smallest graphitic clusters which arose as a side effect of oxidation in acids [57]. Besides the observed changes in the characteristics of the D and G bands, the composites also showed significant differences in the intensity of the D' band. In turn, the variation in the ratio of intensity of the D and D' bands I_D/I_D' (Fig S2) indicate changes in the dominant types of defects present in the samples [60]. The higher values present for unmodified composite CF/PyC points out the dominance of sp^3 defects, while lower values observed for samples after modification with CNT suggest a higher proportion of vacancy defects and grain boundaries [60].

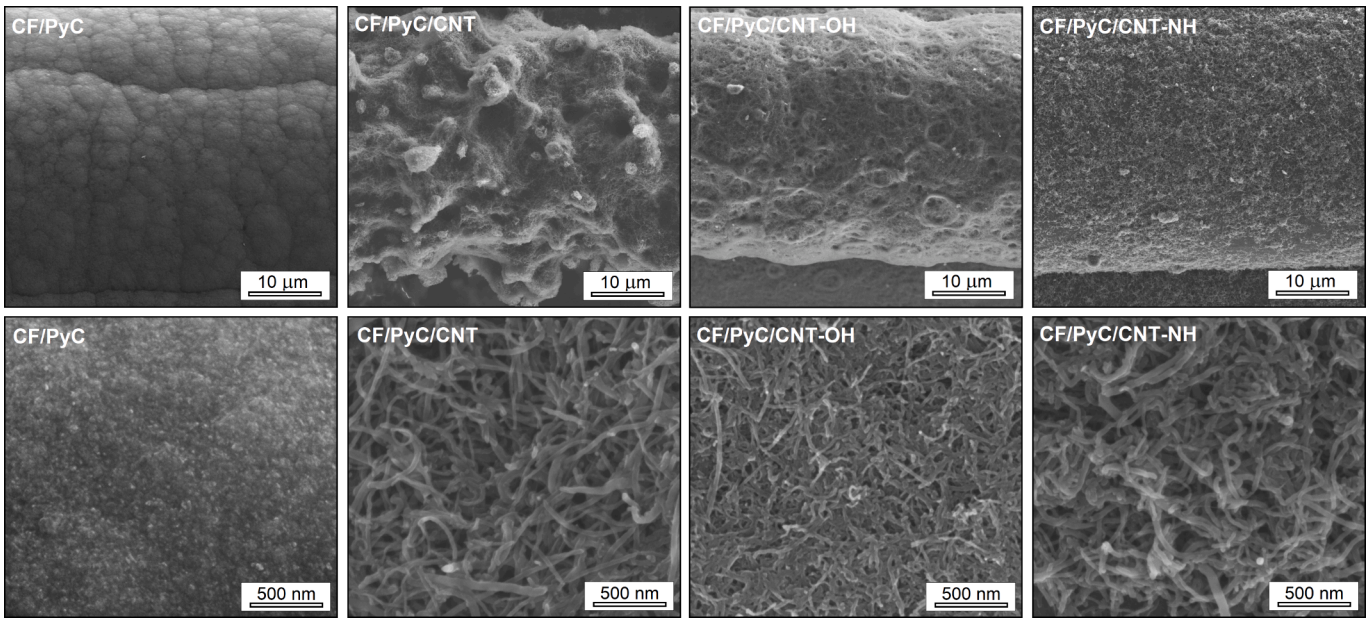

Fig. 4. SEM images of C–C composites subjected to spray coating with various types of CNT. Magnification: upper row – 5000×; lower row – 100,000×.

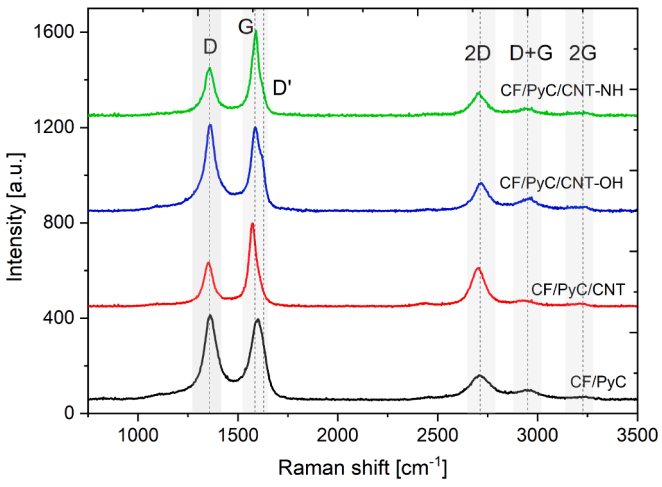

Fig. 5. Raman spectra of C–C composites before and after modification with different carbon nanotubes. The spectra were normalized with reference to the G band.

3.2.1.3. X-ray photoelectron spectroscopy. The presence of functional groups and structural defects on the surface of composite rods were studied using XPS spectroscopy. The C1s, O1s and N1s core level spectra of the as-received CF/PyC composites and CF/PyC after modification using different types of CNT are shown in Figs. 6 and S3. The C1s peak (Fig. 6 A–D) was fitted with the six components assigned to C=C sp^2 bonds (284.4 eV), sp^3 carbon structural defects (285.0 eV), hydroxyl bonds (286.5 eV), carbonyl bonds (287.8 eV), carboxylic groups (289.2 eV), and $\pi \rightarrow \pi^*$ satellite component (290.8 eV) [61,62]. The O1s region was fitted with two lines corresponding to the carboxyl and hydroxyl groups at 533.6 eV and 532.3 eV. In turn, the position of the nitrogen line (Fig. S3) suggests the presence of $–NH_2$ and NHC=O species. The chemical composition of the surface of the tested composites is shown in Table 2.

The blank CF/PyC composite was characterized by the 56.1 % content of sp^2 carbon, and a quite high, 9.7 % content of oxygen present in the form of functional groups on the surface of the pyrocarbon. No nitrogen was detected in this sample. The modification of the CF/PyC composite with pristine CNT resulted in an increase up to 60.5 % in the sp^2 carbon content, and a significant reduction to 1.7 % in the concentration of oxygen. In the same time, the concentration of sp^3 defective carbon decreased, which consistently evidences the more ordered structure of CNT as compared to pyrolytic carbon in CF/PyC. For the CF/PyC/CNT-OH sample, the use of carbon nanotubes oxidized in a mixture of acids resulted in a significant decrease in sp^2 hybridized carbon and an increase in the concentration of defects, which is evidenced by the increase in sp^3 hybridized bonds (Table 2). Also, the total amount of oxygen on the surface of CF/PyC/CNT-OH increased to 14.3 %, more than eight times more than in the CF/PyC/CNT sample. The O/C ratio was highest for this electrode among all tested samples. The deconvolution of the C1s line indicates the major contribution of functional groups in order of –OH (7.4 %), –COOH (4.6 %) and –C=O (3.0 %). In turn, the modification of CNT with ethylenediamine (CF/PyC/CNT-NH) caused a decrease in the number of oxygen groups, especially C–OH, C–O–C and O–C=O at the expense of the appearance of nitrogen functional groups $–NH_2$ and NHC=O [63].

The sp^2 carbon forms the graphitic structure of the CNT sidewalls, while sp^3 carbon atoms and functional groups constitute structural defects of the nanotube walls, therefore the total content of sp^2 carbon can be used as a measure of the structural integrity and structural order of the CNT [64]. The variations in the total content of sp^2 bonded carbon corresponding to the applied modification methods are depicted in Fig. 7. For the samples, the sp^2 carbon percentage was 59.4, 74.8, 47.5 and 58.2 % for CF/PyC, CF/PyC/CNT, CF/PyC/CNT-OH and CF/PyC/CNT-NH respectively, which demonstrates very good consistency with A_D/A_G Raman ratio trends and strengthens the primary conclusions about the structural disorder of the samples. The lowest sp^2 content for the sample oxidized in a mixture of acids (CF/PyC/CNT-OH) indicated a strongly disturbed structure of the CNT-OH due to the strong oxidants used during the chemical functionalization process [59]. Interestingly, the use of a multi-stage amidisation treatment seemed to lead to a partial regeneration of the graphitic character of nanotubes, probably as a result of the removal of highly defective graphitic nanoclusters, which was also confirmed by the results of Raman spectroscopy (Fig. 5).

3.2.2. Electrochemical properties

The cyclic voltammetry of the composite rod electrodes in model artificial cerebrospinal fluid was performed in order to study the effect of applied CNT modifications on the charge injection mechanisms and to

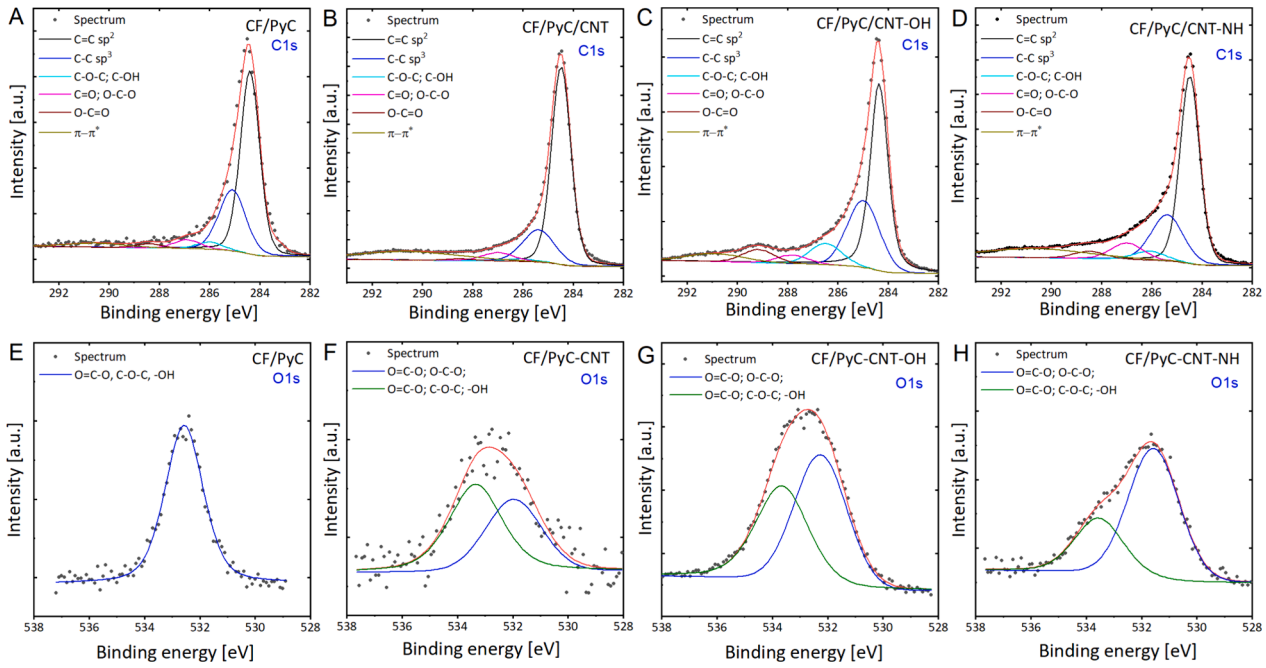

Fig. 6. XPS spectra of C–C composites before and after the spray coating with CNT. Deconvoluted C1s peaks for (A) CF/PyC, (B) CF/PyC/CNT, (C) CF/PyC/CNT-OH and (D) CF/PyC/CNT-NH. Deconvolution O1s peaks for (E) CF/PyC, (F) CF/PyC/CNT, (G) CF/PyC/CNT-OH and (H) CF/PyC/CNT-NH.

Table 2
XPS Surface chemical composition of C–C composites before and after modification with different types of CNT.

XPS Line	C1s						O1s		N1s	O/C
Bonds/groups	C=C (sp^2)	C–C (sp^3)	C–OH	C=O	O–C=O	π → π*	C=O; O–C=O	C–O–C; –COOH; C–OH	–NH_2; NHC=O	–
CF/PyC	56.1	23.1	2.8	3.4	1.6	3.3	9.7	0.0	0.0	0.11
CF/PyC/CNT	60.5	16.6	1.4	4.5	1.0	14.3	0.8	0.9	0.1	0.02
CF/PyC/CNT-OH	42.5	23.2	7.4	3.0	4.6	5.0	7.6	6.7	0.0	0.17
CF/PyC/CNT-NH	45.8	18.5	3.7	6.6	3.0	12.4	3.5	1.5	5.0	0.06

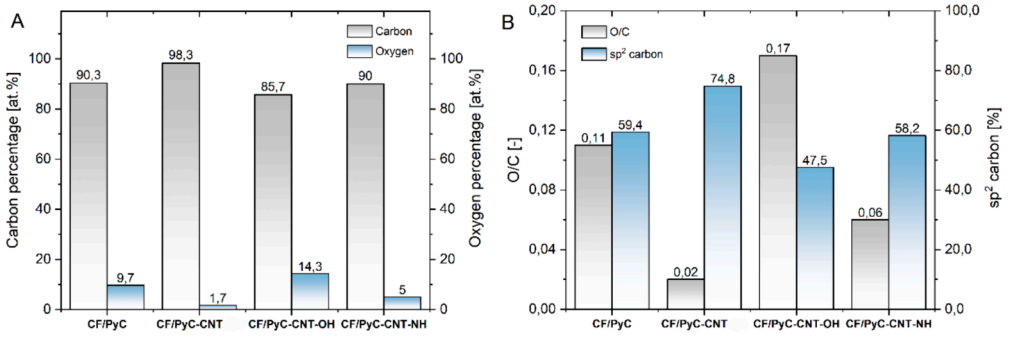

Fig. 7. (A) Surface atomic percentage of carbon and oxygen as determined from XPS. (B) O/C ratio and sp^2 carbon percentage of composites coated with various types of nanotubes.

assess the water windows of electrodes, limiting the range of voltages which can be safely applied in biological systems without causing electrolysis of water. The recorded voltammograms of CF/PyC electrodes after the modification with various types of CNT and reference platinum wire electrode are shown in Fig. 8. The boundary exponential tails visible on all voltammograms mark the hydrogen and oxygen evolution reactions at negative and positive potentials, respectively. These voltages are defined as a water window range of the electrode – V_{ww}, and its values limits the maximal potentials which can be reached at the electrode–electrolyte without causing electrolysis of water at the equilibrium conditions. Here it should be stressed out that because of that DBS simulation consist of short, charge balanced pulses and whole system is burdened with Ohmic and overpotential losses, the actual applied voltage (V_{app}) to the electrodes during stimulation may exceed the values of V_{ww} without necessarily causing the electrolysis of water [44,45]. The Pt wire electrode was characterized by a water window potential range of from −0.72 to 1.23 V, while carbon electrodes showed a significantly widened V_{ww} range between −1.63 to 1.41 V for unmodified CF/PyC, and approximately −1.55 to 1.26 V for all composites after modification with nanotubes. A slight decrease in V_{ww} after deposition of nanotubes was caused by the abundance of active sites on their surface – defects and functional groups, which can be

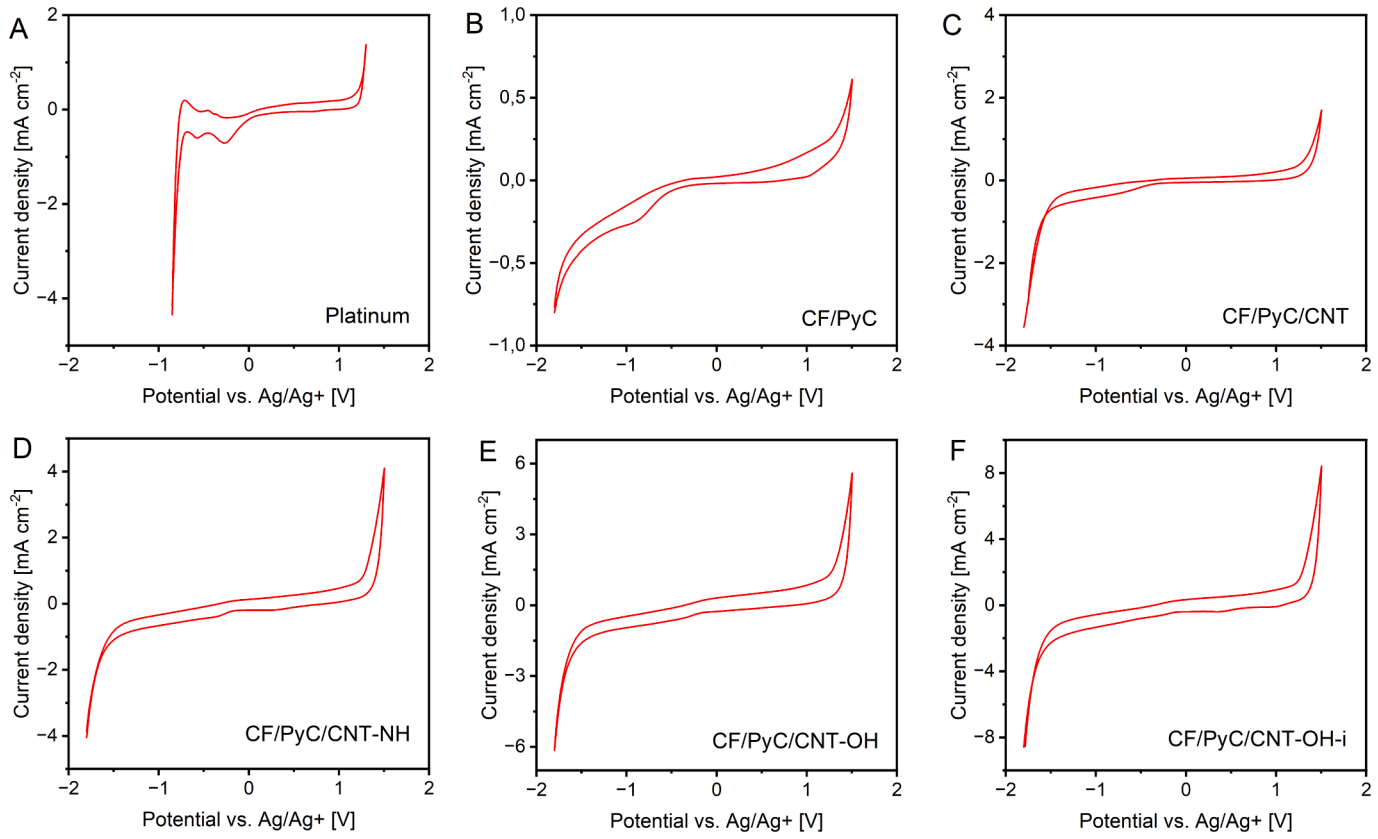

Fig. 8. Cyclic voltammograms of the all materials in an artificial cerebrospinal fluid solution recorded at a 100 mV/s scan rate. (A) Platinum, (B) CF/PyC, (C) CF/PyC/CNT, (D) CF/PyC/CNT-NH, (E) CF/PyC/CNT-OH, (F) CF/PyC/CNT-OH-i (sample with increased amount of CNT).

electrocatalytically active in electrolysis of water. Nonetheless, no significant influence of CNT's surface functional groups was noted on the V_{ww} potential ranges of carbon composites. The exact values of estimated water windows for all materials are shown in Fig. 9 A [44].

Excluding the water electrolytic peaks, carbon electrodes showed predominantly capacitive behavior, with a minor contribution from reversible faradaic processes related to reduction and oxidation of functional groups on the surface of the carbon. The redox peaks from these reactions were more pronounced in the case of non-modified CF/PyC electrodes, while after modification with CNT, their presence was strongly masked by capacitive current components. Notably, the contribution of Faradaic processes was significantly smaller in the case of carbon electrodes as compared to platinum electrodes, which is particularly advantageous since it involves less disruption of the biochemistry in stimulated neural tissue [45].

The cathodic charge storage capacity (CSC_C) corresponds to total charge transferred during cathodic sweep, and its value is frequently reported as a comparative measure, approximating the charge injection capacity of neural stimulation electrodes [43]. The measured values of CSC_c for the obtained electrodes are shown in Fig. 9 B. The reference platinum wire electrode exhibited a CSC_c of 4.12 mC cm^{-2}, and unmodified CF/PyC electrode showed a value of 1.34 mC cm^{-2}. The surface

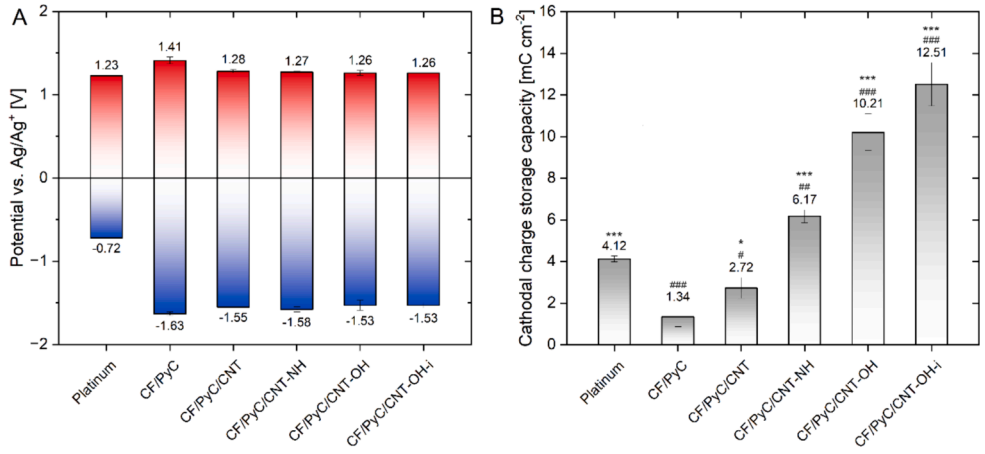

Fig. 9. (A) Water window potential range – V_{ww}, and (B) cathodal charge storage capacity CSC_c of the composite rod electrodes. The CSC_c are presented as a mean ± SD obtained from 3 to 4 measurements for each sample. Statistical analysis was performed with one-way ANOVA and Duncan's post hoc test. $^{*}p < 0.05$, and $^{***}p < 0.001$ vs. CF/PyC; $^{\#}p < 0.05$, $^{\#\#}p < 0.01$ and $^{\#\#\#}p < 0.001$ vs. Platinum.

treatment of composites caused a pronounced increase in CSC_c up to 2.72, 6.17, 10.21 mC cm^{-2} for modifications with neat CNT, CNT-NH, and CNT-OH, respectively. Moreover, we tried to increase the amount of nanotubes deposited on the surface of composite rods by prolonging the spray deposition and using a higher amount of CNT-OH suspension (0.8 ml instead of 0.5 ml), and these samples are denoted CF/PyC/CNT-OH-i. Such treatment resulted in further enhancement of capacitive properties of electrodes, and caused an increase in CSC_c up to 12.51 mC cm^{-2}. Remarkably, this stands for a more than threefold improvement of CSC_c as compared to platinum, and a greater than ninefold improvement as compared to the unmodified CF/PyC composite electrode. The enhanced CSC_c was a direct result of the extensive surface area of carbon nanotubes causing a significant increase in the double layer capacity of electrodes, and thus increasing their charge injection capabilities. This is confirmed by the highest recorded value of CSC_c observed for carbon nanotubes subjected to oxidization treatment (CNT-OH), which, due to morphological and structural disorder, were characterized by the largest specific area of 508.3 m^2 g^{-1}. Enhanced charge storage capacity of such electrodes, as well as their wide range of water window potentials allows for injection of larger portions of charge during a single stimulation pulse, without causing harmful biochemical reactions in neural tissue.

Electrochemical impedance spectroscopy was performed in order to gain further insight into the electrical performance of electrodes, and recorded spectra are shown in Figs. 10 and 11. The shape of the obtained Nyquist plots indicate predominantly capacitive behavior of electrodes without a significant contribution of interfacial charge transfer processes. The spectra were fitted with an equivalent circuit shown in the inset of Fig. 10, consisting of three elements: R_s – corresponding to summary series resistance of the electrodes, connection and electrolyte; CPE_{dl} – constant phase element modeling the non-ideal behavior of double layer capacity of electrode–electrolyte interface; Z_w – a short Wartburg element, modeling the minor contribution of impedance of a finite-length diffusion, which can be attributed to a mass transport due to the migration of ions [65,66]. The measured series resistance R_s was relatively similar for all materials and ranged from 63.9 to 85.4 Ω. The reference unmodified CF/PyC composite electrode was characterized by the lowest R_s of 63.9 Ω, while the modification with all types of carbon nanotubes resulted in a slight increase in the resistance. The type of nanotubes used for the modification showed no statistically significant effect on the series resistance of electrodes.

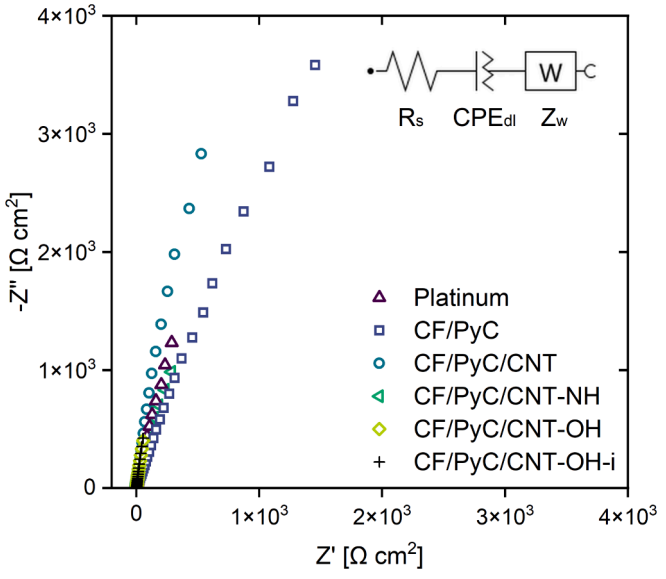

Fig. 10. EIS Nyquist plot of the electrodes in an artificial cerebrospinal fluid solution. The inset shows the equivalent circuit used for the fitting of the spectra.

The double layer capacitance of the electrodes were estimated from CPE parameters using Eq. (1) proposed by Hsu and Mansfeld [67], and its values are of high importance for the performance of stimulation electrodes, as C_{dl} directly contributes to charge injection capacity through a capacitive mechanism.

$$C = Y_0 \left(\omega''_{max}\right)^{n-1} \quad (1)$$

where Y_0 is the characteristic capacitive parameter of CPE, ω''_{max} is the frequency for the maximum of the imaginary part of the impedance, and n is an exponent parameter of CPE.

The platinum wire electrode showed double layer capacitance of 159.6 μF cm^{-2}, while for CF/PyC we recorded 25.7 μF cm^{-2}. Notably, the modification with carbon nanotubes increased capacitance up to 77.6, 152.7, 416.7 and 487.1 μF cm^{-2} for CNT, amidized CNT, CNT-OH, and CNT-OH-i (with increased density of CNT), which corelate with the results obtained from CV. The values of the n exponent defining deviation from the capacitive behavior of CPE, and Z_w comprising contribution of diffusion impedance are both illustrated in Table 3 summarizing all the fitting parameters.

In the case of recording neural electrodes, one of the most important parameters is a signal-to-noise ratio (SNR), which is directly influenced by the magnitude of present thermal noise, which scales with the impedance of an electrode. The impedance at 1 kHz $|Z|_{1kHz}$ is considered as a standard comparative parameter for recording electrodes, and for the Pt wire and CF/PyC electrodes we noted 241.3 Ω (168.9 Ω cm^{-2}) and 898.3 Ω (228.1 Ω cm^{-2}), while after the modification with CNT-OH-i its value decreased to 80.4 Ω (22.2 Ω cm^{-2}). The recorded impedances $|Z|_{1kHz}$ for other types of modifications are summarized in Table 4, while the full Bode plot showing the dependence of impedance on frequency is shown in Fig. 11 A. Another important parameter of recording electrodes is a cut-off frequency $f_{cut\text{-}off}$, which is defined as a frequency at which the magnitude of the signal decreases by 3 dB with reference to the signal transfer in the pass-band [43]. The value of this parameter can be estimated from the Bode plot of phase shift (Fig. 11B) at the angle of −45°, and physically it outlines the transition in the behavior of the electrode from resistive to capacitive character. The neat CF/PyC composite rod electrode exhibited the highest $f_{cut\text{-}off} = 14$ kHz, which was significantly higher than that for the reference Pt wire with $f_{cut\text{-}off} = 1.9$ kHz. In turn, all electrodes after modification had significantly decreased cut-off frequencies, and the best performance was achieved for the CF/PyC/CNT-OH-i electrode with a mean $f_{cut\text{-}off}$ of 0.16 kHz. The obtained values of cut-off frequency and impedance at 1 kHz clearly indicate enhanced recording characteristics of electrodes surface modified with CNT.

The obtained results clearly show a highly positive impact of modification of surface of CF/PyC nanocomposite electrodes with CNT, and the essence of this enhancement was related to increased double layer capacitance of electrodes. The type of nanotubes used had a major impact on both C_{dl} and CSC_c, and it was shown that CNT with hydroxyl groups was most effective, the amidized CNT exhibited moderate effectiveness, while non-functionalized CNT produced a significantly weaker improvement. Most likely, the observed effect on the electrochemical performance of electrodes was related predominantly to the extensive specific surface area and microporosity of carbon nanotubes induced by the chemical treatment, as evidenced by the BET measurements.

3.2.3. *Biological properties*

The chemical composition of the surface of carbon electrodes exerts a significant influence on the biological response of the neural tissue. The biosafety of the composites as electrode material for neural stimulation and recording were investigated in a human neuronal-like model employing human neuroblastoma SH-SY5Y cells. This cell line is a widely accepted in vitro model for testing potential neurotoxicity of various compounds and materials [68], thanks to its catecholaminergic

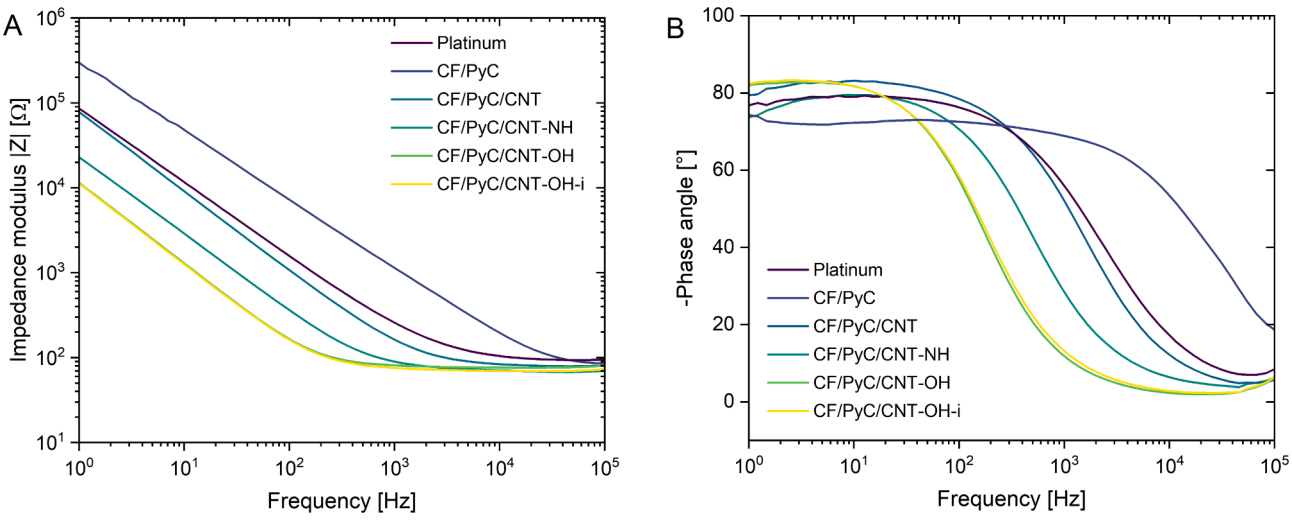

Fig. 11. EIS Bode plots of electrodes in artificial cerebrospinal fluid solution. (A) Impedance modulus, (B) phase shift.

Table 3
Summary of the fitting parameters extracted from EIS data. The results are presented as a mean ± SD obtained from 3 to 4 measurements for each sample. Statistical analysis was performed with one-way ANOVA and Duncan's post hoc test. $^{**}p < 0.01$ and $^{***}p < 0.001$ vs. CF/PyC; $^{\#\#}p < 0.01$, and $^{\#\#\#}p < 0.001$ vs. Platinum.

Sample	R_s [Ω]	C_{dl} [μF cm^{-2}]	n [–]	Z_w (Y_0) [mS s$^{1/2}$]
Platinum	85.4 ± 5.3***	159.6 ± 8.3**	0.89 ± 0.02**	0.6 ± 0.6
CF/PyC	63.9 ± 4.7$^{\#\#\#}$	25.7 ± 8.0$^{\#\#}$	0.81 ± 0.01$^{\#\#}$	1.0 ± 0.1
CF/PyC/CNT	82.2 ± 4.6**	77.6 ± 20.7	0.91 ± 0.03**	2.6 ± 3.6
CF/PyC/CNT-NH	75.5 ± 6.7$^{*,\#}$	152.7 ± 51.2**	0.89 ± 0.04**	2.8 ± 2.3
CF/PyC/CNT-OH	78.2 ± 1.8**	416.7 ± 50.8$^{***,\#\#\#}$	0.93 ± 0.03***	7.9 ± 8.5
CF/PyC/CNT-OH-i	75.3 ± 6.0$^{*,\#}$	487.1 ± 65.3$^{***,\#\#\#}$	0.94 ± 0.02***	8.0 ± 3.4

Table 4
Summary of the electrical parameters of the electrodes. The results are presented as a mean ± SD obtained from 3 to 4 measurements for each sample. Statistical analysis was performed with one-way ANOVA and Duncan's post hoc test. $^{*}p < 0.05$, $^{**}p < 0.01$ and $^{***}p < 0.001$ vs. CF/PyC; $^{\#}p < 0.05$, $^{\#\#}p < 0.01$, and $^{\#\#\#}p < 0.001$ vs. Platinum.

Sample	Potential window [V]	Cathodic CSC [mC cm^{-2}]	C_{dl} (EIS) [μF cm^{-2}]	$\|Z\|_{1kHz}$ [Ω cm^{-2}]	$f_{cut-off}$ [kHz]
Platinum	(−0.72)–1.23	4.12 ± 0.14***	159.6 ± 8.3**	168.9 ± 17.9***	1.90 ± 0.02***
CF/PyC	(−1.63)–1.41	1.34 ± 0.47$^{\#\#\#}$	25.7 ± 8.0$^{\#\#}$	228.1 ± 53.9$^{\#\#\#}$	14.00 ± 4.99$^{\#\#\#}$
CF/PyC/CNT	(−1.55)–1.28	2.72 ± 0.50$^{*,\#}$	77.6 ± 20.7	39.7 ± 2.1***	1.20 ± 0.21***
CF/PyC/CNT-NH	(−1.58)–1.27	6.17 ± 0.31$^{***,\#\#}$	152.7 ± 51.2**	21.1 ± 1.8***	0.33 ± 0.17***
CF/PyC/CNT-OH	(−1.53)–1.26	10.21 ± 0.89$^{***,\#\#\#}$	416.7 ± 50.8$^{***,\#\#\#}$	24.6 ± 3.5***	0.18 ± 0.05***
CF/PyC/CNT-OH-i	(−1.53)–1.26	12.51 ± 1.0$^{***,\#\#\#}$	487.1 ± 65.3$^{***,\#\#\#}$	22.2 ± 1.6***	0.16 ± 0.01***

phenotype it is also a common cellular model for Parkinson's disease [69]. However, it should be kept in mind that this cell line is of tumor origin and could contain various cell population like neuroblast- (N-type) and epithelial- (S-type) like [70]. Nevertheless, the used for the present study SH-SY5Y cells seems to be in prevalence of N-type, as could be assumed by morphological observations (loose surface adherence, elongated shape with neurites) [48] and by showed in our previous work sensitivity of these cells to dopaminergic neurotoxins like MPP+ or 6-OHDA [71,72]. A quantitative biosafety assessment was made by the release of cytotoxic marker LDH after 24 and 48 h of incubation with the samples, and the results are shown in Fig. 12. The two-way ANOVA analysis of LDH release levels did not show a significant difference in cytotoxicity between control cells and cells in contact with any of the tested C–C composites at both of the studied time intervals. The DIC imaging (Fig. 12 A–E) revealed that in the control group, 48 h after seeding, most cells were adhered to the surface of PS well had elongated neurites, and some cells with a rounded shape were loosely attached to the surface. The latter ones could be cells in the process of cell division, or some of them could also be apoptotic (Fig. 12 A). No significant differences compared to the control wells were observed for cells growing in contact with the C–C composites, which demonstrate a lack of negative effects on cells of the tested materials (Fig. 12). The performed tests did not find any detrimental impact of any of the experimental C–C composite electrodes on SH-SY5Y cell viability, as confirmed by DIC images and biochemical measurement of LDH release. In turn, in the case of modification of C–C composites with oxidized carbon nanotubes with hydroxyl/carboxylic groups (CF/PyC/CNT-OH), greater adhesion of nerve cells to the electrode surface can be observed than in other samples (Fig. 12D, arrows). This may be due to the presence of hydroxyl and carboxyl groups on the surface of the composites, which improve the wettability of the surface and thus increase the adhesion of neural cells to the material surface [51,34]. Since the used cellular model for preliminary biological testing is of tumor origin [68,69,70], it will be crucial in the future to test the probes in more physiological models like rodent derived primary neuronal cell cultures or in hiPSC-derived neurons.

4. Conclusion

In this paper, we present novel hybrid C–C composites obtained by the CVD method with direct heating of carbon fibers, modified with carbon nanotubes as a potential electrode material for neural tissue stimulation and recording. In particular, the study focused on analyzing the influence of applied chemical functionalization of carbon nanotubes

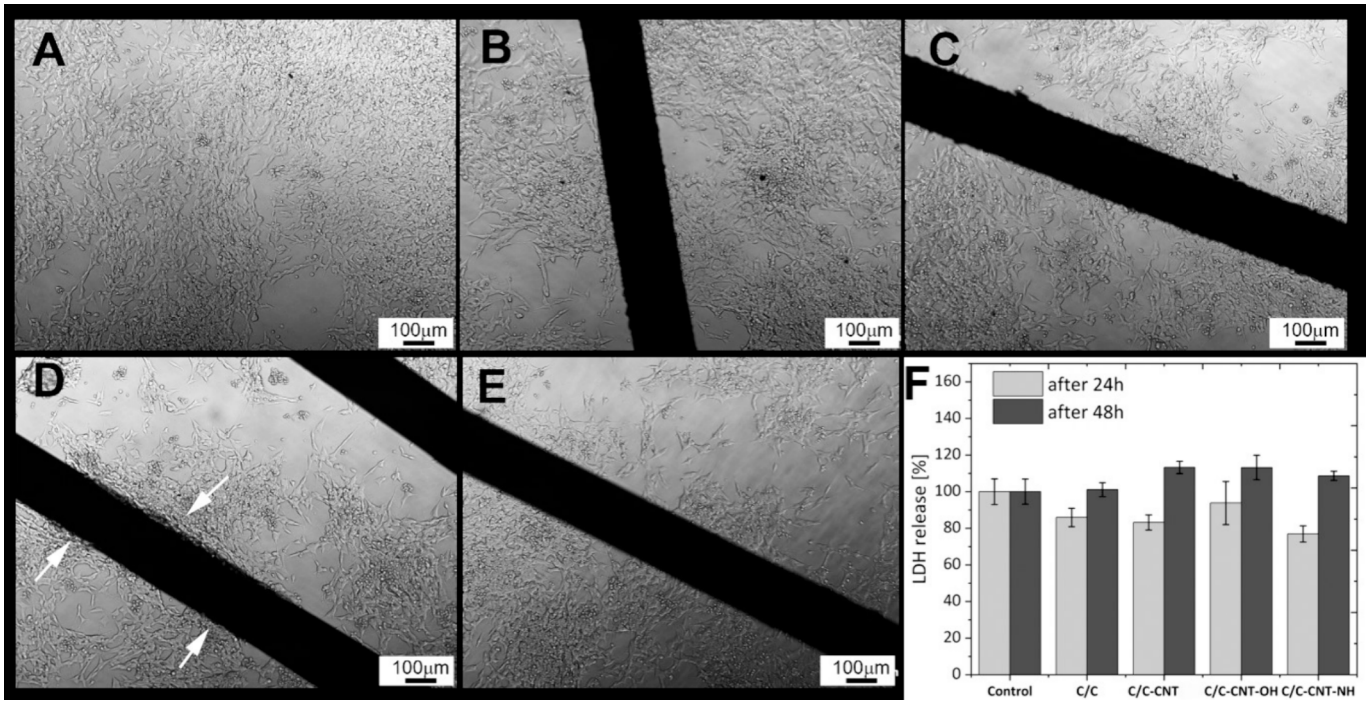

Fig. 12. Differential interference contrast (DIC) images of SH-SY5Y cells in contact with (A) PS-negative control, (B) CF/PyC, (C) CF/PyC/CNT, (D) CF/PyC/CNT-OH, (E) CF/PyC/CNT-NH composite rods. Images were acquired 48 h after cell seeding. (F) Quantitative biosafety assessment of materials using cytotoxicity LDH release biochemical assay. The data were normalized to the control group and are presented as a mean S.E.M. Statistical analysis was performed with two-way ANOVA and Duncan's post hoc test.

on the physicochemical, electrochemical, and biological characteristics of the electrodes.

The obtained composite electrodes coated with carbon nanotubes exhibited significantly improved performance as compared to unmodified C–C composite, and also compared to platinum wire electrode. The enhanced stimulation properties included improved charge injection capability, as evidenced by enlarged CSC_c up to 12.51 mC cm^{-2} due to increased double layer capacity (C_{dl} = 487.1 µF cm^{-2}) resulting from the increased electrochemically active surface area and abundance of active sites on the surface of the nanotubes. Moreover, the electrodes demonstrated improved recording parameters such as decreased impedance at 1 kHz ($|Z|_{1kHZ}$ = 21.1 Ω cm^{-2}), and a lower cut-off frequency ($f_{cut\text{-}off}$ = 0.16 kHz). The chemical treatment of CNT used for surface coating of electrodes was revealed to have a major influence on the performance of electrodes, and this was probably mostly due to the differences in the specific surface area and defect density in the nanotubes. The best results were obtained for CF/PyC/CNT-OH electrodes, prepared using nanotubes subjected to the oxidization treatment in a mixture of strong acids, after which a significant increase in surface area was noted. The preliminary investigation of the biosafety of the electrodes for neural stimulation and recording was carried out using a human neuronal-like model employing human neuroblastoma SH-SY5Y cells, measuring the LDH release biochemical assay, and assessing the morphology of the cells after the contact with materials. The performed test did not show a negative impact of materials on the biological response of cells. The obtained results indicate the high potential of carbon fiber/pyrocarbon/carbon nanotube composites as materials for electrodes for neural stimulation and recording. Future directions of study should focus on obtaining electrodes with desired specific shapes and further evaluation of biological safety, both in vitro and *in vivo* tests.

CRediT authorship contribution statement

Marcel Zambrzycki: Writing – review & editing, Writing – original draft, Validation, Methodology, Investigation. **Ryszard Wielowski:** Writing – original draft, Methodology, Investigation. **Maciej Gubernat:** Investigation. **Danuta Jantas:** Writing – original draft, Methodology, Investigation. **Beata Paczosa-Bator:** Methodology. **Aneta Fraczek-Szczypta:** Writing – review & editing, Writing – original draft, Validation, Supervision, Methodology, Investigation, Funding acquisition, Formal analysis, Conceptualization.

Declaration of competing interest

The authors declare that they have no known competing financial interests or personal relationships that could have appeared to influence the work reported in this paper.

Data availability

Data will be made available on request.

Acknowledgements

This research was funded in whole by National Science Centre, Poland, grant number: UMO-2020/39/B/ST5/02126. For the purpose of Open Access, the author is required to deposit the submitted manuscript to an institutional repository and apply the CC-BY public copyright license to submitted version arising from this submission.

Appendix A. Supplementary material

Supplementary data to this article can be found online at https://doi.org/10.1016/j.apsusc.2024.160713.

References

[1] R.C. Brown, A.H. Lockwood, B.R. Sonawane, Neurodegenerative diseases: an overview of environmental risk factors, Environ. Health Perspect. 113 (2005) 1250–1256, https://doi.org/10.1289/ehp.7567.

[2] R.N.L. Lamptey, B. Chaulagain, R. Trivedi, A. Gothwal, B. Layek, J. Singh, A review of the common neurodegenerative disorders: current therapeutic approaches and the potential role of nanotherapeutics, Int. J. Mol. Sci. 23 (2022) 1851, https://doi.org/10.3390/ijms23031851.

[3] H. Chi, H.-Y. Chang, T.-K. Sang, Neuronal cell death mechanisms in major neurodegenerative diseases, Int. J. Mol. Sci. 19 (2018) 3082, https://doi.org/10.3390/ijms19103082.

[4] K. McFarthing, S. Buff, G. Rafaloff, B. Fiske, L. Mursaleen, R. Fuest, R.K. Wyse, S.R. W. Stott, Parkinson's disease drug therapies in the clinical trial pipeline: 2023 update, J. Parkinsons. Dis. 13 (2023) (2023) 427–439, https://doi.org/10.3233/JPD-239901.

[5] P. Hickey, M. Stacy, Deep brain stimulation: a paradigm shifting approach to treat Parkinson's disease, Front. Neurosci. 10 (2016), https://doi.org/10.3389/fnins.2016.00173.

[6] A.M. Lozano, N. Lipsman, H. Bergman, P. Brown, S. Chabardes, J.W. Chang, K. Matthews, C.C. McIntyre, T.E. Schlaepfer, M. Schulder, Y. Temel, J. Volkmann, J.K. Krauss, Deep brain stimulation: current challenges and future directions, Nat. Rev. Neurol. 15 (2019) 148–160, https://doi.org/10.1038/s41582-018-0128-2.

[7] M. Lamoš, M. Bočková, S. Goldemundová, M. Baláž, J. Chrastina, I. Rektor, The effect of deep brain stimulation in Parkinson's disease reflected in EEG microstates, Npj Park. Dis. 9 (2023) 63, https://doi.org/10.1038/s41531-023-00508-x.

[8] M.S. Okun, Deep-brain stimulation for Parkinson's disease, N. Engl. J. Med. 367 (2012) 1529–1538, https://doi.org/10.1056/NEJMct1208070.

[9] J.K. Krauss, N. Lipsman, T. Aziz, A. Boutet, P. Brown, J.W. Chang, B. Davidson, W. M. Grill, M.I. Hariz, A. Horn, M. Schulder, A. Mammis, P.A. Tass, J. Volkmann, A. M. Lozano, Technology of deep brain stimulation: current status and future directions, Nat. Rev. Neurol. 17 (2021) 75–87, https://doi.org/10.1038/s41582-020-00426-z.

[10] E. Kolaya, B.L. Firestein, Deep brain stimulation: challenges at the tissue-electrode interface and current solutions, Biotechnol. Prog. 37 (2021), https://doi.org/10.1002/btpr.3179.

[11] M. Gulino, D. Kim, S. Pané, S.D. Santos, A.P. Pêgo, Tissue response to neural implants: the use of model systems toward new design solutions of implantable microelectrodes, Front. Neurosci. 13 (2019), https://doi.org/10.3389/fnins.2019.00689.

[12] U.A. Aregueta-Robles, A.J. Woolley, L.A. Poole-Warren, N.H. Lovell, R.A. Green, Organic electrode coatings for next-generation neural interfaces, Front. Neuroeng. 7 (2014), https://doi.org/10.3389/fneng.2014.00015.

[13] T. Hyakumura, U. Aregueta-Robles, W. Duan, J. Villalobos, W.K. Adams, L. Poole-Warren, J.B. Fallon, Improving deep brain stimulation electrode performance in vivo through use of conductive hydrogel coatings, Front. Neurosci. 15 (2021), https://doi.org/10.3389/fnins.2021.761525.

[14] P.R. Patel, H. Zhang, M.T. Robbins, J.B. Nofar, S.P. Marshall, M.J. Kobylarek, T.D. Y. Kozai, N.A. Kotov, C.A. Chestek, Chronic in vivo stability assessment of carbon fiber microelectrode arrays, J. Neural Eng. 13 (2016) 066002, https://doi.org/10.1088/1741-2560/13/6/066002.

[15] Z. Aqrawe, J. Montgomery, J. Travas-Sejdic, D. Svirskis, Conducting polymers as electrode coatings for neuronal multi-electrode arrays, Trends Biotechnol. 35 (2017) 93–95, https://doi.org/10.1016/j.tibtech.2016.06.007.

[16] S. Carli, M. Bianchi, E. Zucchini, M. Di Lauro, M. Prato, M. Murgia, L. Fadiga, F. Biscarini, Electrodeposited PEDOT: nafion composite for neural recording and stimulation, Adv. Healthc. Mater. 8 (2019), https://doi.org/10.1002/adhm.201900765.

[17] Y. Qi, S.-K. Kang, H. Fang, Advanced materials for implantable neuroelectronics, MRS Bull. 48 (2023) 475–483, https://doi.org/10.1557/s43577-023-00540-5.

[18] M.L. Huffman, B.J. Venton, Carbon-fiber microelectrodes for in vivo applications, Analyst. 134 (2009) 18–24, https://doi.org/10.1039/B807563H.

[19] Y. Lee, C. Kong, J.W. Chang, S.B. Jun, Carbon-fiber based microelectrode array embedded with a biodegradable silk support for in vivo neural recording, J. Korean Med. Sci. 34 (2019), https://doi.org/10.3346/jkms.2019.34.e24.

[20] M. Xia, B.N. Agca, T. Yoshida, J. Choi, U. Amjad, K. Bose, N. Keren, S. Zukerman, M.J. Cima, A.M. Graybiel, H.N. Schwerdt, Scalable, flexible carbon fiber electrode thread arrays for three-dimensional probing of neurochemical activity in deep brain structures of rodents, Biosens. Bioelectron. 241 (2023) 115625, https://doi.org/10.1016/j.bios.2023.115625.

[21] M. Hejazi, W. Tong, M.R. Ibbotson, S. Prawer, D.J. Garrett, Advances in carbon-based microfiber electrodes for neural interfacing, Front. Neurosci. 15 (2021), https://doi.org/10.3389/fnins.2021.658703.

[22] F. Vitale, S.R. Summerson, B. Aazhang, C. Kemere, M. Pasquali, Neural stimulation and recording with bidirectional, soft carbon nanotube fiber microelectrodes, ACS Nano. 9 (2015) 4465–4474, https://doi.org/10.1021/acsnano.5b01060.

[23] S. Zhao, G. Li, C. Tong, W. Chen, P. Wang, J. Dai, X. Fu, Z. Xu, X. Liu, L. Lu, Z. Liang, X. Duan, Full activation pattern mapping by simultaneous deep brain stimulation and fMRI with graphene fiber electrodes, Nat. Commun. 11 (2020) 1788, https://doi.org/10.1038/s41467-020-15570-9.

[24] L. Lu, L. Liang, K. Teh, Y. Xie, Z. Wan, Y. Tang, The electrochemical behavior of carbon fiber microelectrodes modified with carbon nanotubes using a two-step electroless plating/chemical vapor deposition process, Sensors. 17 (2017) 725, https://doi.org/10.3390/s17040725.

[25] M.A. Hejazi, W. Tong, A. Stacey, A. Soto-Breceda, M.R. Ibbotson, M. Yunzab, M. I. Maturana, A. Almasi, Y.J. Jung, S. Sun, H. Meffin, J. Fang, M.E.M. Stamp, K. Ganesan, K. Fox, A. Rifai, A. Nadarajah, S. Falahatdoost, S. Prawer, N.V. Apollo, D.J. Garrett, Hybrid diamond/ carbon fiber microelectrodes enable multimodal electrical/chemical neural interfacing, Biomaterials. 230 (2020) 119648, https://doi.org/10.1016/j.biomaterials.2019.119648.

[26] A. Fraczek-Szczypta, N. Kondracka, M. Zambrzycki, M. Gubernat, P. Czaja, M. Pawlyta, P. Jelen, R. Wielowski, D. Jantas, Exploring CVD method for synthesizing carbon-carbon composites as materials to contact with nerve tissue, J. Funct. Biomater. 14 (2023) 443, https://doi.org/10.3390/jfb14090443.

[27] M. Vafaiee, R. Mohammadpour, M. Vossoughi, E. Asadian, M. Janahmadi, P. Sasanpour, Carbon nanotube modified microelectrode array for neural interface, Front. Bioeng. Biotechnol. 8 (2021), https://doi.org/10.3389/fbioe.2020.582713.

[28] M. Zhang, K. Liu, L. Xiang, Y. Lin, L. Su, L. Mao, Carbon nanotube-modified carbon fiber microelectrodes for in vivo voltammetric measurement of ascorbic acid in rat brain, Anal. Chem. 79 (2007) 6559–6565, https://doi.org/10.1021/ac0705871.

[29] C. Boehler, T. Stieglitz, M. Asplund, Nanostructured platinum grass enables superior impedance reduction for neural microelectrodes, Biomaterials. 67 (2015) 346–353, https://doi.org/10.1016/j.biomaterials.2015.07.036.

[30] C. Boehler, D.M. Vieira, U. Egert, M. Asplund, NanoPt—a nanostructured electrode coating for neural recording and microstimulation, ACS Appl. Mater. Interfaces. 12 (2020) 14855–14865, https://doi.org/10.1021/acsami.9b22798.

[31] Z. Zhao, R. Gong, L. Zheng, J. Wang, In vivo neural recording and electrochemical performance of microelectrode arrays modified by rough-surfaced AuPt alloy nanoparticles with nanoporosity, Sensors. 16 (2016) 1851, https://doi.org/10.3390/s16111851.

[32] C. Jiang, L. Li, H. Hao, Carbon nanotube yarns for deep brain stimulation electrode, IEEE Trans. Neural Syst. Rehabil. Eng. 19 (2011) 612–616, https://doi.org/10.1109/TNSRE.2011.2165733.

[33] A. Kunisaki, A. Kodama, M. Ishikawa, T. Ueda, M.D. Lima, T. Kondo, N. Adachi, Carbon-nanotube yarns induce axonal regeneration in peripheral nerve defect, Sci. Rep. 11 (2021) 19562, https://doi.org/10.1038/s41598-021-98603-7.

[34] A. Kunisaki, A. Kodama, M. Ishikawa, T. Ueda, M.D. Lima, T. Kondo, N. Adachi, Oxidation-treated carbon nanotube yarns accelerate neurite outgrowth and induce axonal regeneration in peripheral nerve defect, Sci. Rep. 13 (2023) 21799, https://doi.org/10.1038/s41598-023-48534-2.

[35] Z.-Q. Liu, X.-Y. Yu, J. Huang, X.-Y. Wu, Z.-Y. Wang, B.-P. Zhu, A review: flexible devices for nerve stimulation, Soft Sci. 4 (2024), https://doi.org/10.20517/ss.2023.36.

[36] K. Liu, Y. Sun, R. Zhou, H. Zhu, J. Wang, L. Liu, S. Fan, K. Jiang, Carbon nanotube yarns with high tensile strength made by a twisting and shrinking method, Nanotechnology. 21 (2010) 045708, https://doi.org/10.1088/0957-4484/21/4/045708.

[37] M. Zhang, K.R. Atkinson, R.H. Baughman, Multifunctional Carbon Nanotube Yarns by Downsizing an Ancient Technology, Science (80-.). 306 (2004) 1358–1361. doi: 10.1126/science.1104276.

[38] X. Lepró, M.D. Lima, R.H. Baughman, Spinnable carbon nanotube forests grown on thin, flexible metallic substrates, Carbon N. Y. 48 (2010) 3621–3627, https://doi.org/10.1016/j.carbon.2010.06.016.

[39] X. Zhao, D. Kong, J. Tao, N. Kong, P. Mota-Santiago, P.A. Lynch, Y. Shao, J. Zhang, Wet twisting in spinning for rapid and cost-effective fabrication of superior carbon nanotube yarns, Adv. Funct. Mater. (2024), https://doi.org/10.1002/adfm.202400197.

[40] S. Forti, L. Lunelli, C. Della Volpe, S. Siboni, L. Pasquardini, A. Lui, R. Canteri, L. Vanzetti, C. Potrich, M. Vinante, C. Pederzolli, M. Anderle, Hemocompatibility of pyrolytic carbon in comparison with other biomaterials, Diam. Relat. Mater. 20 (2011) 762–769, https://doi.org/10.1016/j.diamond.2011.03.026.

[41] W. Ze, T. Wen-sheng, Ye-Xia, Z. Ming, L. Xiao-ping, Q. Jian-guo, Y. Xiao-Hong, Preparation of anticoagulant PyC biomaterials with super-hydrophobic surface, J. Appl. Biomater. Funct. Mater. 16 (2018) 125–131, https://doi.org/10.1177/2280800017753315.

[42] T. l, S. C, Blood wettability of haemocompatible carbon-based materials, J. Adv. Chem. Eng. 07 (2017), https://doi.org/10.4172/2090-4568.1000179.

[43] C. Boehler, S. Carli, L. Fadiga, T. Stieglitz, M. Asplund, Tutorial: guidelines for standardized performance tests for electrodes intended for neural interfaces and bioelectronics, Nat. Protoc. 15 (2020) 3557–3578, https://doi.org/10.1038/s41596-020-0389-2.

[44] E.K. Brunton, B. Winther-Jensen, C. Wang, E.B. Yan, S. Hagh Gooie, A.J. Lowery, R. Rajan, In vivo comparison of the charge densities required to evoke motor responses using novel annular penetrating microelectrodes, Front. Neuroeng. 08 (2015), https://doi.org/10.3389/fneng.2015.00005.

[45] S.F. Cogan, Neural stimulation and recording electrodes, Annu. Rev. Biomed. Eng. 10 (2008) 275–309, https://doi.org/10.1146/annurev.bioeng.10.061807.160518.

[46] S.A. Mirdehghan, Fibrous polymeric composites, in: Eng. Polym. Fibrous Mater, Elsevier, 2021, pp. 1–58. doi: 10.1016/B978-0-12-824381-7.00012-3.

[47] R.J. Meier, On art and science in curve-fitting vibrational spectra, Vib. Spectrosc. 39 (2005) 266–269, https://doi.org/10.1016/j.vibspec.2005.03.003.

[48] A. Fraczek-Szczypta, D. Jantas, F. Ciepiela, J. Grzonka, Graphene oxide-conductive polymer nanocomposite coatings obtained by the EPD method as substrates for neurite outgrowth, Diam. Relat. Mater. 102 (2020) 107663, https://doi.org/10.1016/j.diamond.2019.107663.

[49] A. Fraczek-Szczypta, E. Menaszek, S. Blazewicz, Some observations on carbon nanotubes susceptibility to cell phagocytosis, J. Nanomater. 2011 (2011) 1–8, https://doi.org/10.1155/2011/473516.

[50] A. Fraczek-Szczypta, E. Menaszek, T.B. Syeda, A. Misra, M. Alavijeh, J. Adu, S. Blazewicz, Effect of MWCNT surface and chemical modification on in vitro cellular response, J. Nanopart. Res. 14 (2012) 1181, https://doi.org/10.1007/s11051-012-1181-1.

[51] A. Fraczek-Szczypta, D. Jantas, F. Ciepiela, J. Grzonka, A. Bernasik, M. Marzec, Carbon nanomaterials coatings – properties and influence on nerve cells response, Diam. Relat. Mater. 84 (2018) 127–140, https://doi.org/10.1016/j.diamond.2018.03.017.

[52] A. Peigney, C. Laurent, E. Flahaut, R.R. Bacsa, A. Rousset, Specific surface area of carbon nanotubes and bundles of carbon nanotubes, Carbon N. Y. 39 (2001) 507–514, https://doi.org/10.1016/S0008-6223(00)00155-X.
[53] E.M. Elsehly, N.G. Chechenin, A.V. Makunin, A.A. Shemukhin, H.A. Motaweh, Surface functionalization of multi-walled carbon nanotubes by ozone and the enhancement of their environmental applications, Nano Exp. 1 (2020) 020023, https://doi.org/10.1088/2632-959X/abaafd.
[54] M. Larsson, A. Hill, John Duffy, Suspension stability; why particle size, zeta potential and rheology are important, Annu. Trans. Nord. Rheol. Soc. 20 (2012) 209–214.
[55] B. Reznik, K. Norinaga, D. Gerthsen, O. Deutschmann, The effect of cooling rate on hydrogen release from a pyrolytic carbon coating and its resulting morphology, Carbon N. Y. 44 (2006) 1330–1334, https://doi.org/10.1016/j.carbon.2005.12.014.
[56] M.S. Dresselhaus, G. Dresselhaus, R. Saito, A. Jorio, Raman spectroscopy of carbon nanotubes, Phys. Rep. 409 (2005) 47–99, https://doi.org/10.1016/j.physrep.2004.10.006.
[57] V. Datsyuk, M. Kalyva, K. Papagelis, J. Parthenios, D. Tasis, A. Siokou, I. Kallitsis, C. Galiotis, Chemical oxidation of multiwalled carbon nanotubes, Carbon N. Y. 46 (2008) 833–840, https://doi.org/10.1016/j.carbon.2008.02.012.
[58] M. Zambrzycki, P. Jeleń, A. Fraczek-Szczypta, Structure and electrical transport properties of electrospun carbon nanofibers/carbon nanotubes 3D hierarchical nanocomposites: effect of the CCVD synthesis conditions, J. Mater. Sci. 57 (2022) 9334–9356, https://doi.org/10.1007/s10853-022-07267-9.
[59] N. Sezer, M. Koç, Oxidative acid treatment of carbon nanotubes, Surf. Interf. 14 (2019) 1–8, https://doi.org/10.1016/j.surfin.2018.11.001.
[60] A. Eckmann, A. Felten, A. Mishchenko, L. Britnell, R. Krupke, K.S. Novoselov, C. Casiraghi, Probing the nature of defects in graphene by raman spectroscopy, Nano Lett. 12 (2012) 3925–3930, https://doi.org/10.1021/nl300901a.
[61] M. Zambrzycki, R. Piech, S.R. Raga, M. Lira-Cantu, A. Fraczek-Szczypta, Hierarchical carbon nanofibers/carbon nanotubes/NiCo nanocomposites as novel highly effective counter electrode for dye-sensitized solar cells: a structure-electrocatalytic activity relationship study, Carbon N. Y. 203 (2023) 97–110, https://doi.org/10.1016/j.carbon.2022.11.047.
[62] A. Benko, M. Nocuń, M. Gajewska, M. Błażewicz, Addition of carbon nanotubes to electrospun polyacrylonitrile as a way to obtain carbon nanofibers with desired properties, Polym. Degrad. Stab. 161 (2019) 260–276, https://doi.org/10.1016/j.polymdegradstab.2019.01.033.
[63] N. Graf, E. Yegen, T. Gross, A. Lippitz, W. Weigel, S. Krakert, A. Terfort, W.E. S. Unger, XPS and NEXAFS studies of aliphatic and aromatic amine species on functionalized surfaces, Surf. Sci. 603 (2009) 2849–2860, https://doi.org/10.1016/j.susc.2009.07.029.
[64] M. Zambrzycki, S. Łoś, A. Fraczek-Szczypta, Structure and electrical transport properties of carbon nanofibres/carbon nanotubes 3D hierarchical nanocomposites: Impact of the concentration of acetylacetonate catalyst, Ceram. Int. 47 (2021) 4020–4033, https://doi.org/10.1016/j.ceramint.2020.09.269.
[65] A. Balakrishnan, K.R.V. Subramanian (Eds.), Nanostructured Ceramic Oxides for Supercapacitor Applications, CRC Press, 2014. doi: 10.1201/b16522.
[66] B. Paczosa-Bator, Ion-selective electrodes with superhydrophobic polymer/carbon nanocomposites as solid contact, Carbon N.Y. 95 (2015) 879–887, https://doi.org/10.1016/j.carbon.2015.09.006.
[67] C.H. Hsu, F. Mansfeld, Technical note: concerning the conversion of the constant phase element parameter Y 0 into a capacitance, Corrosion. 57 (2001) 747–748, https://doi.org/10.5006/1.3280607.
[68] L. Lopez-Suarez, S. Al Awabdh, X. Coumoul, C. Chauvet, The SH-SY5Y human neuroblastoma cell line, a relevant in vitro cell model for investigating neurotoxicology in human: focus on organic pollutants, Neurotoxicology. 92 (2022) 131–155, https://doi.org/10.1016/j.neuro.2022.07.008.
[69] H. Xicoy, B. Wieringa, G.J.M. Martens, The SH-SY5Y cell line in Parkinson's disease research: a systematic review, Mol. Neurodegener. 12 (2017) 10, https://doi.org/10.1186/s13024-017-0149-0.
[70] J. Kovalevich, D. Langford, Considerations for the use of SH-SY5Y neuroblastoma cells in neurobiology, In (2013:) 9–21, https://doi.org/10.1007/978-1-62703-640-5_2.
[71] D. Jantas, A. Greda, S. Golda, M. Korostynski, B. Grygier, A. Roman, A. Pilc, W. Lason, Neuroprotective effects of metabotropic glutamate receptor group II and III activators against MPP(+)-induced cell death in human neuroblastoma SH-SY5Y cells: the impact of cell differentiation state, Neuropharmacology. 83 (2014) 36–53, https://doi.org/10.1016/j.neuropharm.2014.03.019.
[72] D. Jantas, J. Chwastek, B. Grygier, W. Lasoń, Neuroprotective effects of necrostatin-1 against oxidative stress-induced cell damage: an involvement of cathepsin D inhibition, Neurotox. Res. 37 (2020) 525–542, https://doi.org/10.1007/s12640-020-00164-6.